Journal of Engineering Physics and Thermophysics, Vol. 83, No. 3, 2010

TEMPERATURE AND STRESS IN A CT3 STEEL PLATE DURING AIR-ARC CUTTING AND WELDING PROCESSES

F. I. Panteleenko and A. Heidari Monfared

UDC 669.1

Although the air-arc cutting process has been widely used in material processing engineering, little is known about the temperature and stress in the air-arc cutting of plates. Here, a three-dimensional finite element model including the material removal and thermal effect of the arc is developed to study the temperature and stress fields of a CT3 steel plate during the air-arc cutting and welding processes. The influences of the air-arc cutting process on the initial stress field and of the welding process on the initial residual stress are of primary importance. It is very important for researchers to clarify the temperature and stresses during welding and cutting processes and to fully understand the mechanism of the influence of cutting and welding on the plate.

Keywords: *welding, residual stress, finite element, numerical simulation.*

Introduction. Air-arc cutting is a process in which metal materials are suddenly and locally heated up, as a result of which they fuse, vaporize, and sublime, by an electrical arc beam and are removed immediately by a compression gas flow. Due to the high efficiency and accuracy of the process, it has been widely used for producing grooves in metal plates, in cutting metal plates or back chipping during the welding process (which can be related to pneumatic chipping), wheel forming process, etc. Welding is a reliable and efficient metal-joining process in the production of many engineering and structural components. The advantage of welding as a joining process includes the high joint efficiency, simple setting, and low fabrication cost. However, during the welding processes, the steep temperature gradients that are present in the area under the electrical arc beam, along with the great changes in the mechanical properties and microstructures, yield nonhomogeneous permanent strains and residual stresses in this area after the process. These stresses may lead to cracking just after the welding and sometimes later, during the intended service life. Particularly, the tensile residual stresses near the weld area generally have adverse effects, causing an increase in stresses, fatigue failure, and brittle fracture. Therefore, an accurate estimation of the welding residual stress would be of a great help for ensuring the safety of the structure. However, this estimation is very difficult because of the complexity of the welding process, which includes localized heating, temperature dependence of material properties, a moving heat source, etc. This paper reports on the thermal simulation of the shielded metal arc welding (SMAW) process for butt-welded plates and air-arc cutting of plates by using the finite element (FE) transient heat transfer analysis. The model of a moving heat source composed of the surface and volumetric heat flux functions is applied to the thermal model in a discontinuous manner, assuming a constant welding speed. The effect of the heat source distribution is investigated. The result shows that the temperature distribution and variation in welded plates are sensitive to the heat source distribution and welding process parameters.

Numerical Simulation. *Finite Element Modeling.* The thermal and thermomechanical processes associated with the welding residual stress evolution during welding can be extremely complex. Rapid arc heating during welding produces a molten weld pool. The pool shape can be largely influenced by the weld metal transfer mode and corresponding fluid-flow dynamics.

During cooling, both rapid solidification within the weld pool and solid-state phase transformation in the weld and heat affected zone occur, depending on the peak temperature and cooling rate. Therefore, numerical simulation of the residual stresses due to welding is required to accurately account for the interactions between heat transfer, metallurgical transformation, and mechanical fields. As no metallurgical (martensite) phase transformation occurs in the low carbon steel used in this work, the volumetric effect on the residual stress evolution due to such a transformation is

Belarussian National Technical University, 65 F. Skorina Ave., Minsk, 220013, Belarus; email: panteleenkofi@mail.ru. Published in Inzhenerno-Fizicheskii Zhurnal, Vol. 83, No. 3, pp. 593–597, May–June, 2010. Original article submitted November 6, 2009.

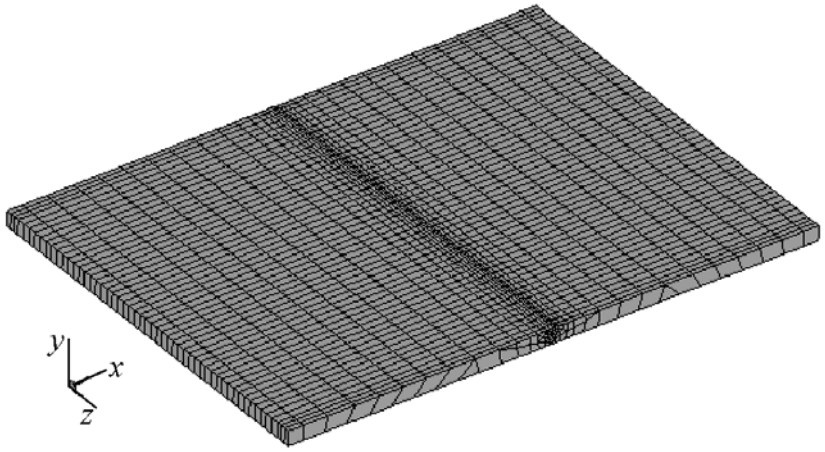

Fig. 1. 3D finite element model of bead-on plate welding.

TABLE 1. Electrical Parameters in Welding and Cutting

Process	I, A	V, V	v, mm/sec
Welding	163–165	22.4	3.2
Cutting	200	22.4	2.2

TABLE 2. Heat Source Parameters in Welding and Cutting (mm)

Process	$2b$	c	f_f	f_r	a_f	a_r
Welding	8	3.5	1.4	0.6	6	10
Cutting	4	5	1.4	0.6	3	6

not considered here. The welding process is a coupled thermomechanical one. The thermal field strongly affects the residual stress field. On the other hand, the stress field has a weak influence on the thermal field. Therefore, the uncoupled analysis is very efficient. To conduct this type of the FE analysis, the three-dimensional uncoupled FE model is developed based on the FE code. The model consists of two parts: a thermal model followed by a mechanical one. The representative 3D thermal elastic-plastic FE model is shown in Fig. 1. A biased mesh is adopted in the transverse direction (x direction) with a finer mesh in the welded region. The model includes 5508 nodes and 3711 elements.

The energy balance equation for *the thermal model* is given by

$$\rho c_p \frac{\partial T}{\partial t}(x, y, z, t) = \nabla q\,(x, y, z, t) + Q\,(x, y, z, t)\,. \tag{1}$$

The Fourier law for an isotropic heat conduction is expressed as

$$q = -k\nabla T\,. \tag{2}$$

For the heat input distribution in the weld region, the most widely accepted double ellipsoidal heat source model presented by Goldak [1] for the spatial heat distribution in a moving reference frame can be calculated on the basis of the following equations:

$$q_f = \frac{6\sqrt{3}\,\eta Q f_f}{\pi\sqrt{\pi}\,a_f bc} \exp\left\{-3\left(\frac{z^2}{a_f^2} + \frac{y^2}{b^2} + \frac{x^2}{c^2}\right)\right\}, \tag{3}$$

$$q_r = \frac{6\sqrt{3}\,\eta Q f_r}{\pi\sqrt{\pi}\,a_r bc} \exp\left\{-3\left(\frac{z^2}{a_r^2} + \frac{y^2}{b^2} + \frac{x^2}{c^2}\right)\right\}, \tag{4}$$

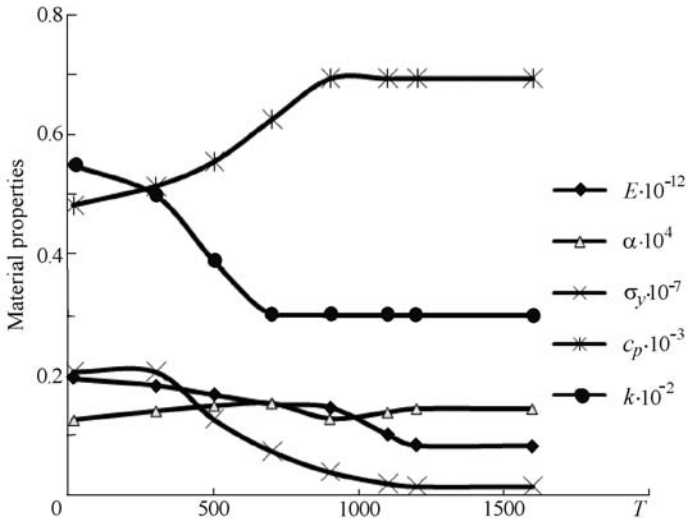

Fig. 2. Temperature dependences of the thermal properties. E, Pa; α, 1/K; σ_y, Pa; c_p, J·kg^{-1}·K^{-1}; k, W·m^{-1}·K^{-1}; T, ^{o}C.

where $Q = UI$, $f_r + f_f = 2$. The heat source is assumed to move through the volume, and the calculated heat is applied to the elements as volumetric heat generation, so that the elements lying on the surface can be used for modeling surface heat convection. The electrical parameters for welding and cutting processes are shown in Table 1, and the numerical values of the heat source parameters for these processes are presented in Table 2.

Mechanical Model. In *the mechanical analysis*, the temperature history obtained from the analysis was used as a thermal loading in the structural model. The thermal stresses and strains can be calculated at each time increment. Moreover, the final state of the residual stresses will be accumulated by the thermal strains and stresses. During simulation, the thermal stresses are calculated from the temperature distributions determined by the thermal model. The residual stresses from each temperature increment are added to the nodal point location to determine the updated behavior of the model before the next temperature increment. The kinematic hardening rule is used, which is an essential feature, since material points typically undergo both loading and unloading in the course of welding and cutting processes.

Material Properties. The isotropic behavior of the material is assumed. The initial temperature of the base metal is equal to 3 ^{o}C. The Poisson ratio is 0.3, and the mass density is 7813 kg/m^3. The convective film boundary condition is applied to all the exposed faces of the base metal, and the heat transfer coefficient is equal to 20 W/(m^2·K). The ambient temperature amounts to 15^{o}C. Other temperature-dependent physical and mechanical properties are shown in Fig. 2.

In the models of both cutting and welding processes, the technique of the "*deactivation/activation element*" is adopted. In the cutting model, which simulates the removal of the material, a thermal flux is focused on the place which should be air-arc cut, and the elements are deactivated as soon as their temperature exceeds the material point. The element is deactivated when the temperature of one integration point is above the material melting point. This means that the temperature, strain, and stress are set to zero as soon as the element is deactivated, and it will no longer be activated in the subsequent air-arc cutting process. In the welding model, during the thermal analysis all the nodes of the deactivated elements in the region of the filler metal (except for those shared with the base metal) are also fixed at ambient temperature prior to the birth of the respective element. The deactivated elements are reactivated sequentially when they come under the influence of the heat source.

Experimental Procedure. The material used in this study is a CT3 plate steel with length, width, and thickness of 90, 134, and 5 mm, respectively. The sequence of weld passes is shown schematically in Fig. 1. The shielded metal arc welding is used in the experiments. The filler metal has a diameter of 4 mm.

Results and Discussion. Figures 3 and 4 present the stresses and temperatures during and after the welding and air-arc cutting processes. The contour band patterns of *the temperature fields* during the air-arc processes in 17 sec are shown in Figs. 3e and f. In these figures, the maximum temperature exceeds the melting point of the base material

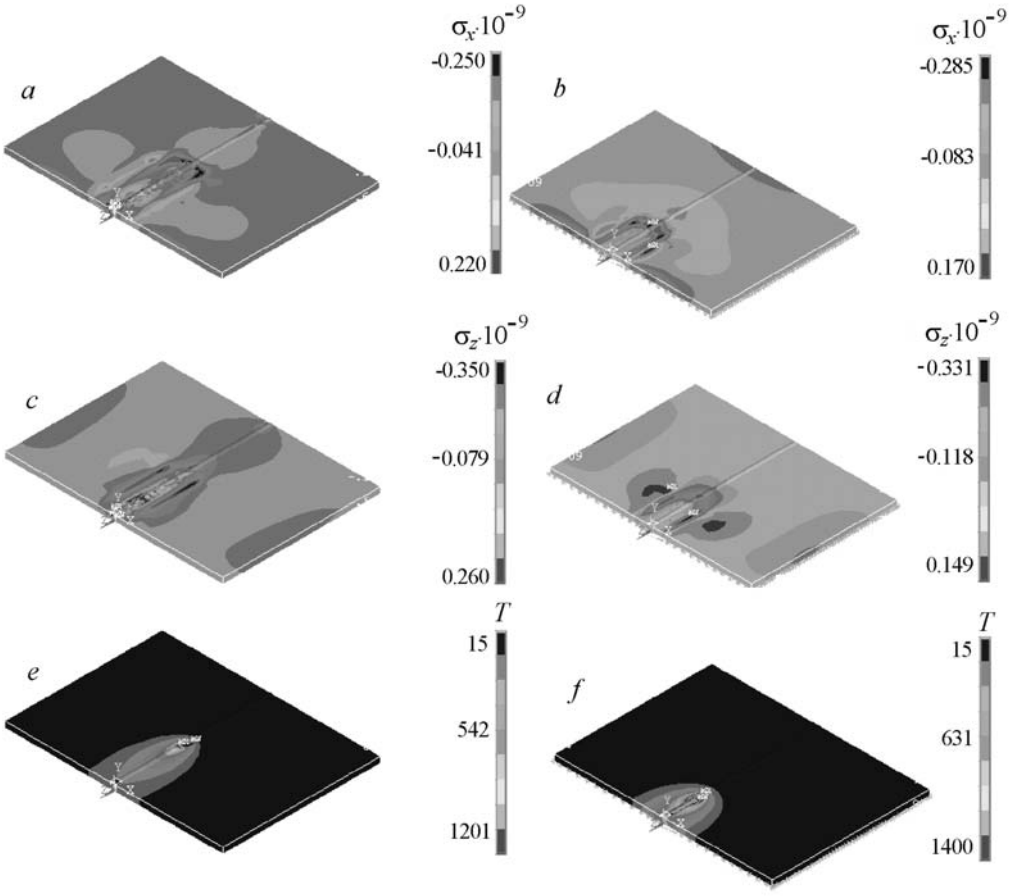

Fig. 3. Evolution of the stresses (a, b, c, and d) and temperature (e and f) during welding (a, c, and e) and air-arc cutting (b, d, and f). σ_x, Pa; σ_z, Pa; T, ^{o}C.

almost as soon as the electrical arc beam is applied to the zone that is to be air-arc cut or welded. A molten pool can be seen in the front of the groove in Figs. 3e and f. Figures 4e and f show the temperature fields when the air-arc cutting and welding have been completed and the groove is distinctly seen.

The evolution of the longitudinal stress is shown in Fig. 3c and d. Due to the heat effect of the arc, the materials under the arc expand in 17 sec from the beginning of the air-arc cutting process (as shown in Figs. 3c and d). However, this expansion is prevented by other surrounding materials that are still at room temperature. Then the materials under the arc generate compression stresses, while the materials around them bear tensile stresses.

In addition, the materials in front of the arc generate compression stresses, which are greater than those for the rear position. This is due to the fact that the arc moves forward, and the front materials achieve greater heat energy. The stresses of the material at the center of the arc are equal to zero, because the elements are deactivated by the program, when their temperatures reach the melting point of the steel. The whole distribution of the stresses is represented by the compression stress in front of the arc, zero compression at the center, and tensile stress on the rear of the arc. Moreover, the heat effects of the arc are focused mainly on the material near or under the arc beam, and the zones far away from the arc generate small stresses. This is due to the fact that the thermal flux during the air-arc cutting process is greatly concentrated.

The air-arc cutting and welding processes terminate in 80 sec, as seen in Figs. 4c and d. The great tensile stresses occur at the places around the groove that have been cooled sufficiently. It can be noted that the heated parts begin to shrink, but they are prevented by the cold parts around them, so that the tensile stress arises there, while in the other parts the compression stress appears. The parts around the new groove are still in the compression stress state.

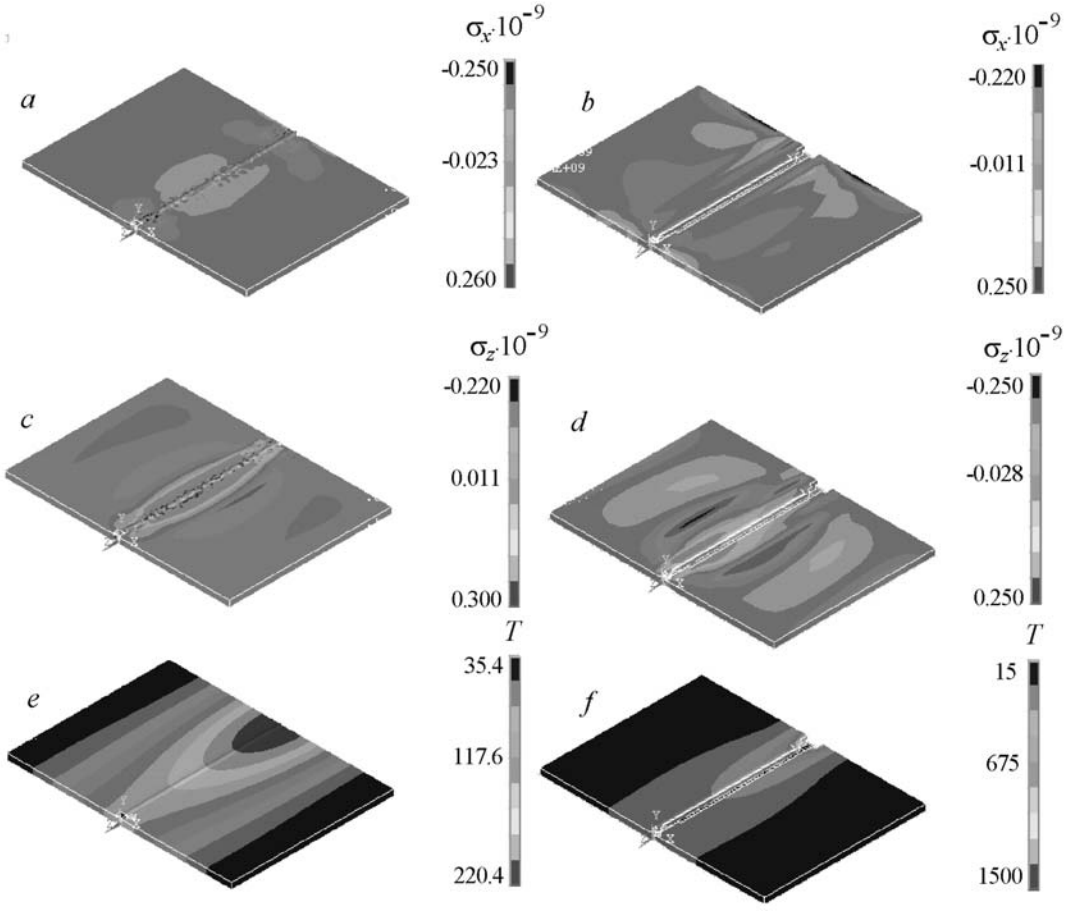

Fig. 4. Evolution of the stresses (a, b, c, and d) and temperature (e and f) after welding (a, c, and e) and air-arc cutting (b, d, and f). σ_x, Pa; σ_z, Pa; T, ^{o}C.

From the above analysis, it can be understood that the evolution of the stress during the air-arc cutting is similar to that for the butting welding process in the same material. The great residual stresses occur near the groove in the plate. The residual stresses in the air-arc cutting process seem also to be similar to those of the butt welding process for flat plates: great tensile stresses occur near a groove, and the maximum of the longitudinal residual stresses is greater than that for the transverse residual stresses. The longitudinal residual stress decreases from the great tensile stress to the compression stress, while the transverse stress decreases down to zero. It is worth noting that, if a plate is to be welded after the air-arc cutting process, greater tensile stress concentration may be induced in engineering practice.

CONCLUSIONS

1. The temperature and stress fields in the air-arc cutting and welding processes for a CT3 steel plate have been successfully studied using the finite element method. The material removal and thermal effects of the arc were considered.

2. It is shown that the temperature fields in the air-arc cutting and welding processes change sharply.

3. The longitudinal residual stress distribution in the air-arc cutting process seems to be similar to that for the butt welding process for flat plates. The great residual tensile stresses occur near a groove, and the longitudinal residual stress decreases from the tensile stress to the compression one.

4. During a cutting process, a high tensile vertical stress arises in front of the arc due to the removal of the material in the arc region.

5. During a welding process, a tensile stress occurs on the rear of the arc due to the concentration effect.

6. The longitudinal residual stresses are higher than the transverse ones.

NOTATION

a_f and a_r, lengths of front and rear ellipsoids, respectively; b and c, half-width and depth of heat source; c_p, specific heat; E, Young's modulus; f_f and f_r, fractions of heat in front and rear ellipsoids; I, welding current; k, thermal conductivity; Q, rate of internal heat generation; q, heat flux; T, temperature; t, time; V, welding voltage; v, welding speed; x, y, z, coordinates; α, thermal expansion coefficient; ρ, density; σ_x and σ_z, transverse and longitudinal residual stresses; σ_y, yield stress. Subscripts: f, front; r, rear.

REFERENCES

1. Jun-Feng Hu, Jian-Guo Yang, Hong-Yuan Fang, Guang-Min Li, Yong Zhang, and Xin Wan, Temperature, stress and microstructure in 10Ni5CrMoV steel plate during air-arc cutting process, *J. Comput. Mater. Sci*., **38**, 631–641 (2007).
2. Chin-Hyung Lee and Kyong-Ho Chang, Three-dimensional finite element simulation of residual stresses in circumferential welds of steel pipe including pipe diameter effects, *J. Mater. Sci. Eng. A*, **487**, 210–218 (2008).
3. P. Akerstrom and M.Oldenburg, Austenite decomposition during press hardening of a boron steel — Computer simulation and test, *J. Mater. Proc. Tech.*, **174**, 399–406 (2006).
4. A. Capriccioli and P. Frosi, Multipurpose ANSYS FE procedure for welding processes simulation, *Journal of Fusion Engineering and Design*, www.elsevier.com/locate/fusengdes (2009).
5. Huajun Zhang, Guangjun Zhang, Chunbo Cai, Hongming Gao, and Lin Wu, Fundamental studies on in-process controlling angular distortion in asymmetrical double-sided double arc welding, *J. Mater. Proc. Tech*., **205**, 214–223 (2008).
6. S. V. Pearce, V. M. Linton, and E. C. Oliver, Residual stress in a thick section high strength T-butt weld, *J. Mater. Sci. Eng. A*, **480**, 411–418 (2008).
7. Dean Deng and Hidekazu Murakawa, Numerical simulation of temperature field and residual stress in multi-pass welds in stainless steel pipe and comparison with experimental measurements, *J. Comput. Mater. Sci*., **37**, 269–277 (2006).
8. Tso-Liang Teng, Chin-Ping Fung, and Peng-Hsiang Chang, Effect of weld geometry and residual stresses on fatigue in butt-welded joints, *Int. J. Pressure Vessels Piping*, **79**, 467–482 (2002).
9. T. B. Brown, T. A. Dauda, C. E. Truman, D. J. Smith, D. Memhard, and W. Pfeiffer, Predictions and measurements of residual stress in repair welds in plates, *Int. J. Pressure Vessels Piping*, **83**, 809–818 (2006).
10. Dean Deng, Hidekazu Murakawa, and Wei Liang, Numerical and experimental investigations on welding residual stress in multi-pass butt-welded austenitic stainless steel pipe, *J. Comput. Mater. Sci.*, **42**, 234–244 (2008).
11. Dean Deng, Hidekazu Murakawa, and Wei Liang, Prediction of welding distortion in a curved plate structure by means of elastic finite element method, *J. Mater. Proc. Tech*., **203**, 252–266 (2008).
12. Tso-Liang Teng, Peng-Hsiang Chang, and Wen-Cheng Tseng, Effect of welding sequences on residual stresses, *J. Comput. Struct.*, **81**, 273–286 (2003).
13. Z. Barsoum and A. Lundback, Simplified FE welding simulation of fillet welds — 3D effects on the formation residual stresses, *J. Eng. Fail. Anal.*, www.elsevier.com/locate/engfailanal (2009).
14. Rui Wang, Jianxun Zhang, Hisashi Serizawa, and Hedekazu Murakawa, Study of welding inherent deformations in thin plates based on finite element analysis using interactive substructure method, *J. Mater. Design*, www.elsevier.com/locate/matdes (2009).